AGU PUBLICATIONS

Geophysical Research Letters

RESEARCH LETTER
10.1002/2015GL065446

Key Points:
- New regional seismic data confirm the supershear rupture during the M_w 6.7 Okhotsk deep earthquake
- The moment-rate function based on a joint inversion has a smooth shape without any temporal gaps
- The M_w 6.7 Okhotsk deep earthquake is more likely a continuous rupture than a triggered doublet

Correspondence to:
Z. Zhan,
zwzhan@gps.caltech.edu

Citation:
Zhan, Z., P. M. Shearer, and H. Kanamori (2015), Supershear rupture in the 24 May 2013 M_w 6.7 Okhotsk deep earthquake: Additional evidence from regional seismic stations, *Geophys. Res. Lett.*, *42*, doi:10.1002/2015GL065446.

Received 19 JUL 2015
Accepted 10 SEP 2015
Accepted article online 14 SEP 2015

Supershear rupture in the 24 May 2013 M_w 6.7 Okhotsk deep earthquake: Additional evidence from regional seismic stations

Zhongwen Zhan[1,2], Peter M. Shearer[1], and Hiroo Kanamori[2]

[1]Institute of Geophysics and Planetary Physics, University of California, San Diego, La Jolla, California, USA, [2]Seismological Laboratory, California Institute of Technology, Pasadena, California, USA

Abstract Zhan et al. (2014a) reported supershear rupture during the M_w 6.7 aftershock of the 2013 M_w 8.3 Sea of Okhotsk deep earthquake, relying heavily on the regional station PET, which played a critical role in constraining the vertical rupture dimension and rupture speed. Here we include five more regional stations and find that the durations of the source time functions derived from these stations are consistent with Zhan et al.'s supershear rupture model. Furthermore, to reduce the nonuniqueness of deconvolution and combine the bandwidths of different stations, we conduct a joint inversion of the six regional stations for a single broadband moment-rate function (MRF). The best fitting MRF, which explains all the regional waveforms well, has a smooth shape without any temporal gaps. The M_w 6.7 Okhotsk deep earthquake is more likely a continuous supershear rupture than a dynamically triggered doublet.

1. Introduction

While most earthquakes' rupture speeds (V_r) are less than the local shear wave (V_S) or Rayleigh wave speeds (V_R), supershear ruptures (i.e., $V_r > V_S$) have been reported for several shallow strike-slip earthquakes (e.g., 1979 Imperial Valley, 1999 Izmit, 2001 Kunlun, 2002 Denali, 2010 Yushu, and 2013 Craig earthquakes) [*Archuleta*, 1984; *Bouchon et al*., 2001; *Bouchon and Vallée*, 2003; *Dunham and Archuleta*, 2004; *Walker and Shearer*, 2009; *Vallée and Dunham*, 2012; *Wang and Mori*, 2012; *Yue et al*., 2013]. Observations and understanding of supershear ruptures have important implications for seismic hazard and earthquake dynamics [*Dunham et al*., 2003; *Xia et al*., 2004; *Dunham*, 2007; *Das*, 2010; *Mello et al*., 2010; *Schmedes et al*., 2010]. For example, *Gabuchian et al*. [2014] show that upward supershear rupture on a thrust fault would enhance the ground shaking by a factor of 2 to 3. Although the physics and conditions of the transition from subshear ($V_r < V_S$) to supershear rupture are not yet fully understood, previous observations and theoretical studies indicate that high prestress and high seismic efficiency (e.g., a simple fault geometry) help promote supershear rupture [*Zhang and Chen*, 2006; *Bouchon et al*., 2010; *Kaneko and Lapusta*, 2010].

The physical mechanism of earthquakes deeper than 300 km is still enigmatic, and the rupture speeds of deep earthquakes appear highly variable [*Frohlich*, 2006; *Houston*, 2007]. For example, the two largest deep earthquakes recorded by modern seismological networks, the 1994 M_w 8.2 Bolivia and 2013 M_w 8.3 Sea of Okhotsk earthquakes, have rupture speeds of ~$0.3V_S$ and ~$0.7V_S$, respectively [*Kikuchi and Kanamori*, 1994; *Silver et al*., 1995; *Antolik et al*., 1996; *Ihmlé*, 1998; *Wei et al*., 2013; *Ye et al*., 2013; *Chen et al*., 2014; *Meng et al*., 2014; *Zhan et al*., 2014b]. *Kuge* [1994] inferred that the 1990 M_w 7.1 Sakhalin deep earthquake ruptured at a supershear speed. By studying the *P* wave directivity effect at both teleseismic and regional stations, *Zhan et al*. [2014a] showed that supershear rupture ($V_r \approx 8$ km/s $\approx 1.4V_S$, local $V_S \approx 5.5$ km/s) occurred during the 24 May 2013 M_w 6.7 Okhotsk earthquake (depth = 642 km), the largest aftershock of the M_w 8.3 Okhotsk event. More specifically, the event ruptured downdip along a steep fault plane dipping at 70° in the SE direction, with a rupture azimuth of about 130°. The horizontal and vertical rupture dimensions are 4 km and 11 km, respectively. The supershear rupture speed indicates highly efficient seismic radiation (i.e., radiation efficiency $\eta_R \approx 1$), which contrasts strongly with the nearly zero radiation efficiency during the Bolivia earthquake ($\eta_R < 0.036$) [*Kanamori et al*., 1998], suggesting more than one rupture mechanism for deep earthquakes [*Zhan et al*., 2014a].

In this paper, we extend the work of *Zhan et al*. [2014a] to address two key questions: (1) The only regional station used in *Zhan et al*. [2014a] is station PET (Figure 1); its longer source time function

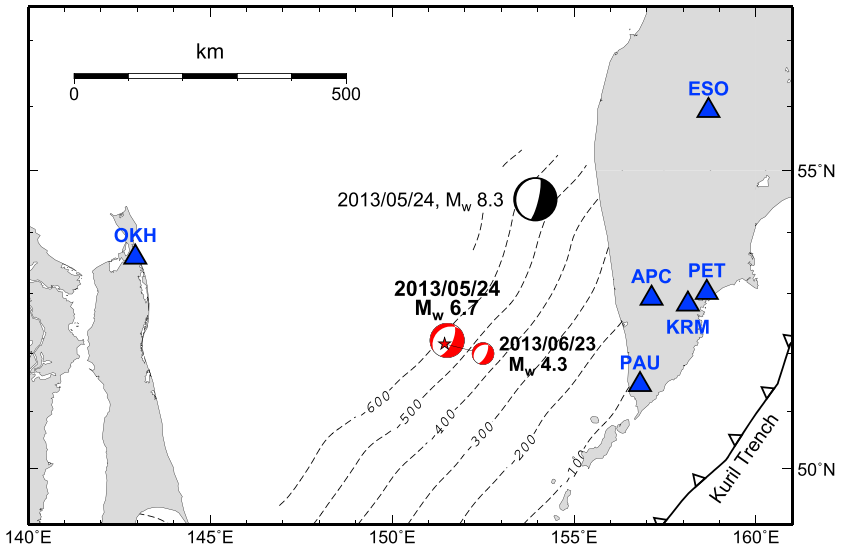

Figure 1. Map of the regional seismic stations (blue triangles). The 2013 Okhotsk M_w 8.3 main shock and M_w 6.7 aftershock are displayed as the black and red beach balls, respectively. The red star connected to the smaller beach ball represents the M_w 4.3 EGF event used in this study. Slab contours from the Slab 1.0 model are shown as dashed lines [*Hayes et al.*, 2012].

(STF) duration than those of the teleseismic stations is largely what constrains the steeply dipping fault geometry and high rupture speed. Would additional regional stations confirm the supershear rupture model? (2) Can we distinguish between a continuous supershear rupture and a doublet with two well-separated subevents? A second subevent dynamically triggered by *P* waves from the first subevent could produce high apparent rupture speed, and this possibility is an important issue because a significant gap in the STF of station PET can be interpreted as two distinct subevents [*Zhan et al.*, 2014a]. However, the nonuniqueness of deconvolution with narrow-band empirical Green's functions (EGFs) limits the robustness of results from a single station. The teleseismic stations provide little additional information regarding the detailed rupture process because their STFs are strongly compressed by the downward rupture directivity and also lack high-frequency energy due to attenuation.

In this paper, we include more regional stations to answer these two questions. Besides the PET station openly available from the Incorporated Research Institutions for Seismology Data Management Center, we obtained data from five more broadband regional stations operated by the Kamchatkan Branch of Geophysical Survey of Russian Academy of Science (Figure 1). All six stations recorded the M_w 6.7 event and its *M* 4.3 aftershock (Figure 2), which serves as the EGF event to correct for path effects. In the next two sections, we will first repeat the procedures for station PET to estimate the STF durations and test whether they are consistent with the supershear rupture model. Then we will take advantage of the broadband signals at multiple stations to estimate a robust broadband moment-rate function (MRF) to address the question of continuous rupture versus a dynamically triggered doublet.

2. Source Time Function Durations

Observed seismograms at the regional stations are convolutions of source and path effects. In particular, wave diffraction along the high-velocity subducting slab produces significant complexities in the upgoing seismic wavefield. For example, *P* waveforms of the M_w 4.3 event at stations KRM and APC display double arrivals separated by 0.5 –1.5 s, which are likely caused by multipathing of the upgoing ray paths (Figure 2). To separate the source parameters from the path effects, we use the waveforms of the M_w 4.3 aftershock as empirical Green's functions (EGFs). *Zhan et al.* [2014a] have demonstrated that the M_w 4.3 event is an ideal EGF event, with small moment but similar depth and focal mechanism as the M_w 6.7 earthquake.

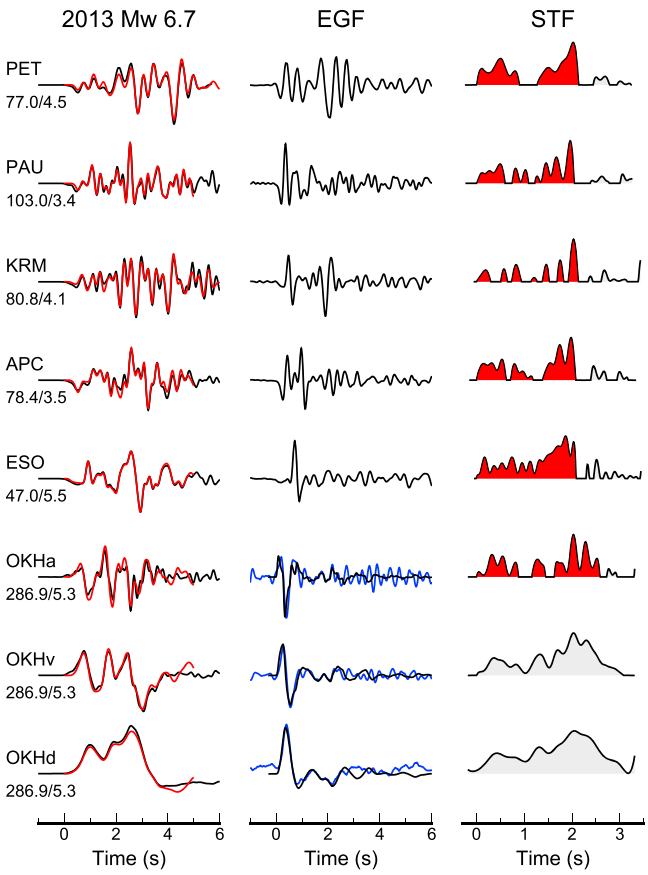

Figure 2. Regional seismic waveforms and deconvolution. The three columns display vertical-component seismograms of the M_w 6.7 earthquake, EGFs, and the deconvolved STFs. To ensure high signal-to-noise ratios and enhance high-frequency energy, we use broadband acceleration seismograms. The black and red traces in the first column are the data and predictions, respectively. The two numbers beneath the station names are azimuths and distances in degrees. In the third column, we show the STF durations defined by the red shading, which includes most of the energy. In the bottom three rows, we display the deconvolution of acceleration (OKHa), velocity (OKHv), and displacement (OKHd) records of station OKH. For OKH, to avoid the long-period noise in the observed EGF seismograms (blue traces), we use synthetic Green's functions (sGF, black traces) calculated with the 1-D velocity model shown in Figure 4.

Following the same procedures as in *Zhan et al.* [2014a], we derive the STFs $x(t)$ by deconvolving the EGFs $u(t)$ from the M_w 6.7 earthquake waveforms $w(t)$ with an optimization-based method in the time domain. The convolution

$$u(t) * x(t) = w(t)$$

where * is a convolution operator, which can be written in a linear matrix form

$$Ux = w$$

where x and w are $n_u \times 1$ and $n_w \times 1$ matrices, U is a $n_w \times n_u$ matrix with each row as a time-shifted $u(t)$. The parameters n_u and n_w are the number of samples of $u(t)$ and $w(t)$. We solve the inverse problem for x by minimizing the L^2 norm of data residuals and model parameters, with a positivity constraint:

$$\text{minimize } \|Ux - w\|_2^2 + \lambda \|x\|_2^2 \text{ , subject to : } x \geq 0$$

where λ is a regularization parameter chosen by the L curve method [e.g., *Aster et al.*, 2011] to ensure reasonably good waveform fits and compact STFs.

The small magnitude of the M_w 4.3 EGF event ensures its simple source process but also limits the frequency band with high signal-to-noise ratios (SNRs); even at the regional stations, the EGFs are still noisy at low frequencies ($f < 0.5$~Hz). To stay consistent with *Zhan et al.* [2014a] and focus on the high-frequency energy

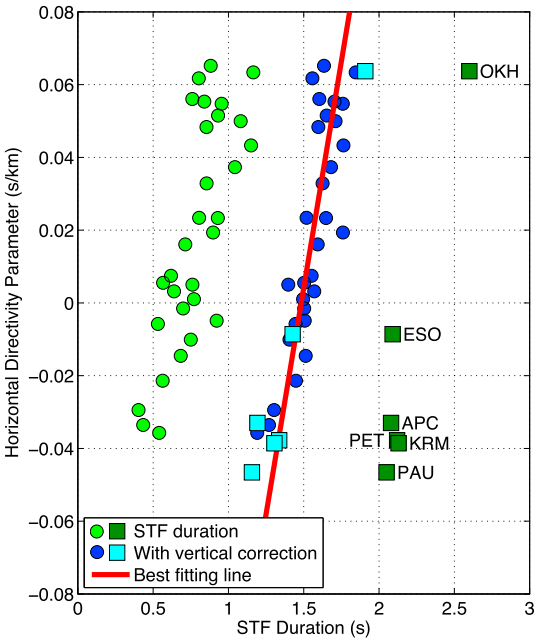

Figure 3. Teleseismic (dots) and regional (squares) STF durations with and without vertical directivity corrections. We assume the same rupture parameters as in *Zhan et al.* [2014a]. The corrected regional STF durations (cyan squares) fall near the same straight line estimated previously from the teleseismic data (blue dots).

that has high SNRs, we conduct the deconvolutions using the broadband acceleration seismograms. Figure 2 shows the deconvolution results. For all six stations, relatively simple and compact STFs convolved with the EGFs produce good fits to the *P* wave acceleration seismograms of the M_w 6.7 earthquake, and station PET is no exception. We measure the STF durations as the segments including most of the energy, shown as the red shaded areas in Figure 2. The five stations to the east of the events, including PET, show similar STF durations (~2.1 s), even though their waveforms are different due to different slab waveform effects. This consistency is expected for their similar azimuths and further demonstrates the effective correction of path effects. OKH is the only station to the west of the source in this study, and it shows a significantly longer STF duration (~2.6 s), as expected for the southeastward rupture directivity.

To test the supershear rupture model more quantitatively, in Figure 3, we plot the STF durations versus the horizontal directivity parameter, which is defined as $x_i(\theta_r) = -\frac{\cos(\theta_i - \theta_r)}{c_P^i}$ for the *i*th station with azimuth θ_i and *P* wave phase velocity $c_P^i = \frac{\alpha}{\sin\phi_i}$. Here ϕ_i is the take-off angle for the *i*th station and α is the *P* wave speed. Because we are not inverting for a new rupture model but testing whether new data are consistent with the previous rupture model, we assume the rupture direction $\theta_r = 130°$, the same as that derived in *Zhan et al.* [2014a]. Compared with the teleseismic STF durations (green dots in Figure 3), all regional STF durations are significantly longer, consistent with the downward rupture along the steeply dipping fault plane. Then we correct the regional STF durations for the vertical rupture dimension H = 11 km, by $\eta_i H$, where $\eta_i = -\frac{\cos\phi_i}{\alpha}$ is the vertical slowness. The corrected STF durations (cyan squares) fall near the predictions from the previous rupture model (red line in Figure 3). Thus, the *P* wave STF durations of the new regional data are consistent with the supershear rupture model. Considering the uncertainties in STF durations, we do not find it necessary to update the rupture model.

3. Joint Inversion for the Moment-Rate Function

The regional STFs, stretched by the downward rupture directivity (STF durations ~ 2.1–2.6 s), provide more details about the rupture process than the compressed teleseismic STFs (durations ~ 0.5–1 s). However, limited by the bandwidths of the *M* 4.3 EGFs, regional STFs are still estimated by deconvolving accelerations and are only well constrained at high frequency (>1 Hz). In other words, the bandwidths of the STFs are mostly constrained by the EGFs, not by the high-SNR records of the M_w 6.7 event. STF broadband features such as peaks and gaps are mostly controlled by the regularization and positivity constraints and have intrinsic nonuniqueness. For example, the STF of station PET has a gap separating two apparent subevents; however, STFs of the other five stations, which supposedly share the same shape, are different (Figure 2).

To retrieve the broadband moment-rate function (MRF), we need to find at least one broadband approximation of the Green's function, with greater bandwidth than the available EGFs. As discussed above, the five stations to the east of the target events show strong waveform complexities due to slab effects, and we do not

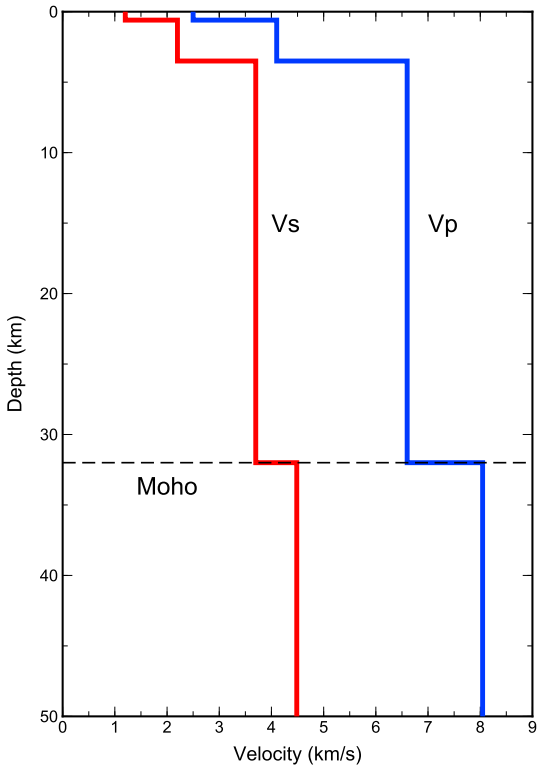

Figure 4. One-dimensional velocity model for station OKH, merged and modified from CRUST 2.0 and PREM. Note that the calculated synthetic seismograms fit the OKH observations well (Figure 2).

have an accurate 3-D velocity model to account for the effects. However, the ray path to station OKH, located to the west of the events, likely avoids the NW dipping high-velocity slab and samples a relatively simple upper mantle. Indeed, the OKH records look relatively simple compared with the other stations (Figure 2). This inspires us to calculate synthetic seismograms to fit OKH's records. We merge the 1-D model near OKH from CRUST 1.0 [*Laske et al.*, 2013] with the PREM upper mantle model [*Dziewonski and Anderson*, 1981], modify the shallow part (Figure 4), and compute synthetic seismograms for the M_w 4.3 event using a frequency-wave number method [*Zhu and Rivera*, 2002]. As shown in the bottom three rows of Figure 2, the OKH waveforms, especially the velocity and displacement records, are fit well by the 1-D synthetics. Therefore, the 1-D model in Figure 4 accurately represents the velocity structure along the ray path to OKH, and the 1-D synthetic Green's function (sGF) can be considered as a good approximation to the true GF. The advantage of replacing the EGF with the sGF in the deconvolution is that the sGF is noise free and has clean broadband information, which is of primary importance in estimating the broadband moment-rate function.

To improve the uniqueness/robustness of the deconvolution, we conduct a joint inversion for the MRF with all six regional stations simultaneously. With the confirmed rupture geometry and speed in the last section, we further assume a unilateral rupture with a constant rupture speed. Then, the individual STFs can be considered as the MRF uniformly stretched by a factor of T_i/τ, where τ is the source duration and T_i is the predicted STF duration for station i. For the joint inversion, we undo the temporal scaling by compressing the data and EGFs/sGF by factors of τ/T_i so that the new STFs are expected to be the same as the MRF for all stations. We use the displacement sGF for station OKH, and acceleration EGFs for the other five stations. Their amplitudes are scaled to be roughly the same so that every station contributes equally to the inversion. The choice of the damping parameter λ is still based on the L curve method, but is found to be much less sensitive due to the better joint constraints. The resulted MRF of the joint inversion is shown in Figure 5. Using this single MRF, we achieve reasonable waveform fits for all stations, which show that the joint inversion helps to overcome the nonuniqueness in individual deconvolutions and combines different stations' bandwidths effectively. With the constraint from the OKH displacement record, the new MRF has more long-period energy than the individual STFs derived from acceleration seismograms (Figure 2), while the high-frequency components of the MRF are still able to fit the high-frequency accelerations of the other five stations.

The new MRF has a smooth shape with no gaps, which is more consistent with a continuous rupture than a dynamically triggered doublet. To further test the maximum allowed gap in the MRF by the regional waveforms, we impose gaps of different widths on the MRF around the position where the PET STF shows the gap and compute the waveform fitting residuals of the joint inversions. As shown in Figure 5, gaps wider than 0.1 s increase the residuals rapidly, mostly due to worsened fits to the OKH displacement data. Furthermore, unrealistic spikes are induced at the edges of the gaps in the MRFs (e.g., green inset in Figure 5, right). When the imposed gap width reaches 0.18 s, the OKH record is not fit at all and its constraints on the long-period MRF properties disappear; hence, the MRF absolute amplitude drops significantly (cyan inset in Figure 5, right). This again demonstrates the critical broadband constraint on the MRF provided by the station OKH. When the gap width reaches 0.36 s, the waveform fits of the other five stations' acceleration data also

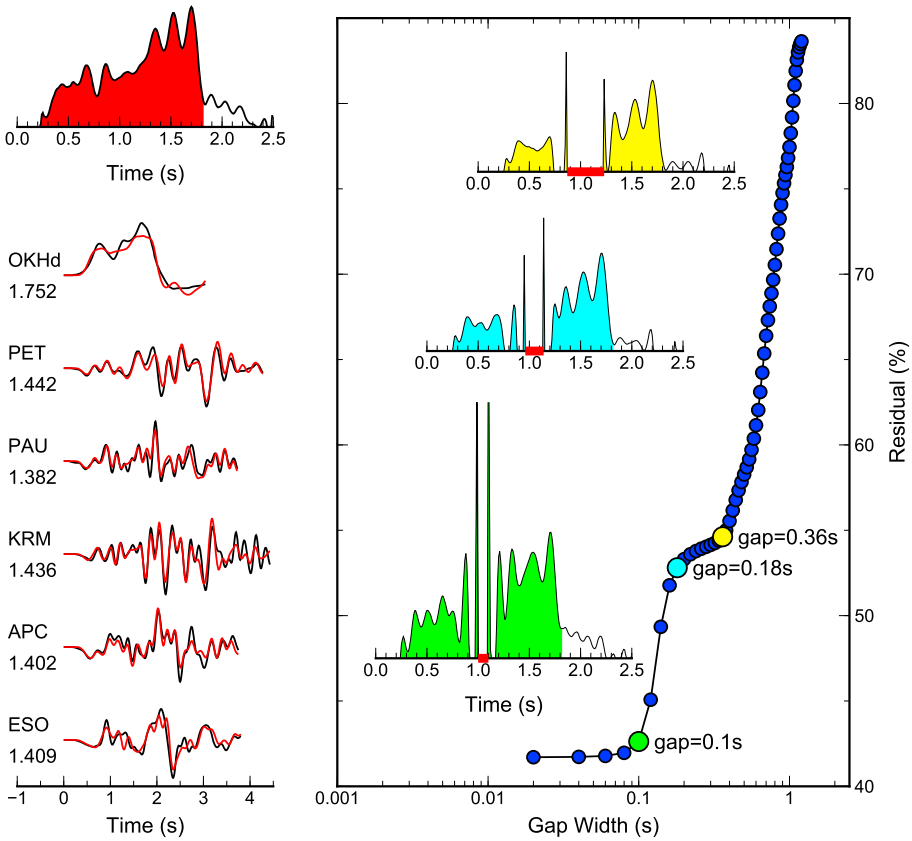

Figure 5. Joint inversion of six regional stations for a single moment-rate function. Except the displacement seismogram of OKH, all other data are in broadband acceleration. All seismograms are plotted in true relative time scales and amplitudes as they are compressed and weighted in the joint inversion. The numbers below the station names are the temporal scaling factors. The black and red traces are the data and predictions, respectively. (top left) The final moment-rate function, with the source duration shaded in red, which includes most of the energy (right column) The residual in percentage versus the imposed gap width around 1.05 s, where the STF using only the PET station shows a gap. When the gap width is larger than 0.1 s, the residual increases rapidly. Unrealistic spikes are induced at the edges of the imposed gaps. The resulting MRFs at three turning points (large green, cyan, and yellow dots) are displayed with the same time and amplitude scales. When the imposed gap increases beyond 0.18 s, the waveform fit of the OKH displacement is too poor to provide long-period constraints, and the absolute MRF amplitudes drop.

degrade significantly. Therefore, the maximum allowed gap in the MRF is less than 0.1 s, much shorter than the total source duration of ~1.5 s. The gap observed in the PET STF is an artifact of the narrow-band data and intrinsic nonuniqueness of deconvolution.

The inversion approach described above assumes a constant rupture velocity and tests for the possibility of rupture gaps defined by gaps (zero values) in the moment-rate function. We also experimented with an alternate model defined by two point sources, in which the second source is triggered by the *P* wave from the first source. We were unable to find any combination of source separation distance and subevent durations that could fit both the regional and teleseismic data. This is not surprising, given that the subevent durations cannot exceed the shortest teleseismic pulse durations for a point source model, and thus the subevents cannot sum to more than twice this duration for regional station observations without introducing a gap in the predicted regional STF records.

4. Conclusions

In this paper, we have shown that the STF durations of the additional regional stations are consistent with the rupture geometry and supershear rupture speed determined in *Zhan et al*. [2014a]. We also conduct joint inversions of all regional stations' waveforms and find that the broadband MRF is relatively smooth and

has no significant gaps. The gap in the STF of station PET is an artifact caused by limited EGF bandwidth and the nonuniqueness of deconvolution. The continuous STF obtained in this paper indicates that the M_w 6.7 event is most likely a continuous supershear rupture and not a dynamically triggered doublet. A continuous rupture and a doublet are physically distinct models. The former has a stress concentration near the advancing edge of the faulting area, while the latter involves static or dynamic stress in the medium that is large enough to trigger another independent event, which is not necessarily connected to the initial event by a contiguous slip surface. However, given the limited resolution of teleseismic data, it would be difficult to distinguish a series of subevents triggered by *P* waves from true supershear rupture. What we can rule out with the smooth MRF that we obtain here is a model where a very localized subevent triggers another well-separated and localized subevent, in which case the MRF would have a distinct gap separating two subevents with high stress drops.

Acknowledgments
Victor Chebrov and Anastasia Chebrova kindly made available to us the broadband data from seismic stations of the Kamchatka Branch of Geophysical Survey, Russian Academy of Science. Incorporated Research Institutions for Seismology (IRIS) provided the seismic data of station PET and the teleseismic stations (http://dx.doi.org/doi:10.7914/SN/IU). We thank two anonymous reviewers for their helpful comments. This work was supported by National Science Foundation grant EAR-111111.

The Editor thanks two anonymous reviewers for their assistance in evaluating this paper.

References

Antolik, M., D. Dreger, and B. Romanowicz (1996), Finite fault source study of the great 1994 deep Bolivia earthquake, *Geophys. Res. Lett.*, *23*(13), 1589–1592, doi:10.1029/96GL00968.

Archuleta, R. J. (1984), A faulting model for the 1979 Imperial Valley earthquake, *J. Geophys. Res.*, *89*(B6), 4559–4585, doi:10.1029/JB089iB06p04559.

Aster, R. C., B. Borchers, and C. H. Thurber (2011), *Parameter Estimation and Inverse Problems*, Elsevier Academic Press, Boston.

Bouchon, M., and M. Vallée (2003), Observation of long supershear rupture during the magnitude 8.1 Kunlunshan earthquake, *Science*, *301*(5634), 824–826.

Bouchon, M., M. P. Bouin, H. Karabulut, M. N. Toksöz, M. Dietrich, and A. J. Rosakis (2001), How fast is rupture during an earthquake? New insights from the 1999 Turkey earthquakes, *Geophys. Res. Lett.*, *28*(14), 2723–2726, doi:10.1029/2001GL013112.

Bouchon, M., H. Karabulut, M.-P. Bouin, J. Schmittbuhl, M. Vallée, R. Archuleta, S. Das, F. Renard, and D. Marsan (2010), Faulting characteristics of supershear earthquakes, *Tectonophysics*, *493*(3–4), 244–253.

Chen, Y., L. Wen, and C. Ji (2014), A cascading failure during the 24 May 2013 great Okhotsk deep earthquake, *J. Geophys. Res. Solid Earth*, *119*, 3035–3049, doi:10.1002/2013JB010926.

Das, S. (2010), Earthquake supershear rupture speeds, *Tectonophysics*, *493*(3–4), 213–215.

Dunham, E. M. (2007), Conditions governing the occurrence of supershear ruptures under slip-weakening friction, *J. Geophys. Res.*, *112*, B07302, doi:10.1029/2006JB004717.

Dunham, E. M., and R. J. Archuleta (2004), Evidence for a supershear transient during the 2002 Denali Fault earthquake, *Bull. Seismol. Soc. Am.*, *94*(6B), S256–S268.

Dunham, E. M., P. Favreau, and J. M. Carlson (2003), A supershear transition mechanism for cracks, *Science*, *299*(5612), 1557–1559.

Dziewonski, A. M., and D. L. Anderson (1981), Preliminary reference Earth model, *Phys. Earth Planet. Inter.*, *25*(4), 297–356.

Frohlich, C. (2006), *Deep Earthquakes*, Cambridge Univ. Press, Cambridge, U. K.

Gabuchian, V., A. J. Rosakis, N. Lapusta, and D. D. Oglesby (2014), Experimental investigation of strong ground motion due to thrust fault earthquakes, *J. Geophys. Res. Solid Earth*, *119*, 1316–1336, doi:10.1002/2013JB010409.

Hayes, G. P., D. J. Wald, and R. L. Johnson (2012), Slab1. 0: A three-dimensional model of global subduction zone geometries, *J. Geophys. Res.*, *117*, B01302, doi:10.1029/2011JB008524.

Houston, H. (2007), Deep earthquakes, in *Treatise on Geophysics*, edited by G. Schubert, pp. 321–350, Elsevier, New York.

Ihmlé, P. F. (1998), On the interpretation of subevents in teleseismic waveforms: The 1994 Bolivia deep earthquake revisited, *J. Geophys. Res.*, *103*(B8), 17,919–17,932, doi:10.1029/98JB00603.

Kanamori, H., D. L. Anderson, and T. H. Heaton (1998), Frictional melting during the rupture of the 1994 Bolivian earthquake, *Science*, *279*(5352), 839–842.

Kaneko, Y., and N. Lapusta (2010), Supershear transition due to a free surface in 3-D simulations of spontaneous dynamic rupture on vertical strike-slip faults, *Tectonophysics*, *493*(3–4), 272–284.

Kikuchi, M., and H. Kanamori (1994), The mechanism of the deep Bolivia earthquake of June 9, 1994, *Geophys. Res. Lett.*, *21*(22), 2341–2344, doi:10.1029/94GL02483.

Kuge, K. (1994), Rapid rupture and complex faulting of the May 12, 1990, Sakhalin deep earthquake: Analysis of regional and teleseismic broadband data, *J. Geophys. Res.*, *99*(B2), 2671–2685, doi:10.1029/93JB02992.

Laske, G., G. Masters, Z. Ma, and M. Pasyanos (2013), Update on CRUST1.0—A 1-degree global model of Earth's crust, *Geophys. Res. Abstracts*, *15*, Abstract EGU2013-2658.

Mello, M., H. S. Bhat, A. J. Rosakis, and H. Kanamori (2010), Identifying the unique ground motion signatures of supershear earthquakes: Theory and experiments, *Tectonophysics*, *493*(3–4), 297–326.

Meng, L., J. P. Ampuero, and R. Bürgmann (2014), The 2013 Okhotsk deep-focus earthquake: Rupture beyond the metastable olivine wedge and thermally controlled rise time near the edge of a slab, *Geophys. Res. Lett.*, *41*, 3779–3785, doi:10.1002/2014GL059968.

Schmedes, J., R. J. Archuleta, and D. Lavallée (2010), Dependency of supershear transition and ground motion on the autocorrelation of initial stress, *Tectonophysics*, *493*(3–4), 222–235.

Silver, P. G., S. L. Beck, T. C. Wallace, C. Meade, S. C. Myers, D. E. James, and R. Kuehnel (1995), Rupture characteristics of the deep Bolivian earthquake of 9 June 1994 and the mechanism of deep-focus earthquakes, *Science*, *268*, 69–69.

Vallée, M., and E. M. Dunham (2012), Observation of far-field Mach waves generated by the 2001 Kokoxili supershear earthquake, *Geophys. Res. Lett.*, *39*, L05311, doi:10.1029/2011GL050725.

Walker, K. T., and P. M. Shearer (2009), Illuminating the near-sonic rupture velocities of the intracontinental Kokoxili *Mw*7.8 and Denali fault *Mw*7.9 strike-slip earthquakes with global *P* wave back projection imaging, *J. Geophys. Res.*, *114*, B02304, doi:10.1029/2008JB005738.

Wang, D., and J. Mori (2012), The 2010 Qinghai, China, earthquake: A moderate earthquake with supershear rupture, *Bull. Seismol. Soc. Am.*, *102*(1), 301–308.

Wei, S., D. Helmberger, Z. Zhan, and R. Graves (2013), Rupture complexity of the*Mw* 8.3 Sea of Okhotsk earthquake: Rapid triggering of complementary earthquakes?, *Geophys. Res. Lett.*, *40*, 5034–5039, doi:10.1002/grl.50977.

Xia, K., A. J. Rosakis, and H. Kanamori (2004), Laboratory earthquakes: The sub-Rayleigh-to-supershear rupture transition, *Science*, *303*(5665), 1859–1861.

Ye, L., T. Lay, H. Kanamori, and K. D. Koper (2013), Energy release of the 2013 *Mw* 8.3 Sea of Okhotsk earthquake and deep slab stress heterogeneity, *Science*, *341*(6152), 1380–1384.

Yue, H., T. Lay, J. T. Freymueller, K. Ding, L. Rivera, N. A. Ruppert, and K. D. Koper (2013), Supershear rupture of the 5 January 2013 Craig, Alaska (*Mw* 7.5) earthquake, *J. Geophys. Res. Solid Earth*, *118*, 5903–5919, doi:10.1002/2013JB010594.

Zhan, Z., D. V. Helmberger, H. Kanamori, and P. M. Shearer (2014a), Supershear rupture in a *Mw* 6.7 aftershock of the 2013 Sea of Okhotsk earthquake, *Science*, *345*(6193), 204–207.

Zhan, Z., H. Kanamori, V. C. Tsai, D. V. Helmberger, and S. Wei (2014b), Rupture complexity of the 1994 Bolivia and 2013 Sea of Okhotsk deep earthquakes, *Earth Planet. Sci. Lett.*, *385*, 89–96.

Zhang, H., and X. Chen (2006), Dynamic rupture on a planar fault in three-dimensional half-space—II. Validations and numerical experiments, *Geophys. J. Int.*, *167*(2), 917–932.

Zhu, L., and L. A. Rivera (2002), A note on the dynamic and static displacements from a point source in multilayered media, *Geophys. J. Int.*, *148*(3), 619–627.